Environment Dependent Trade-Offs in Eco-Driving with Driver Preference Integration for Electric Vehicles

Samia Qamar[1], Peter Hubbard[1], Will Midgley[2], James Fleming[1]

***Abstract*—Eco-driving optimisation offers significant potential for reducing energy consumption in electric vehicles; however, its effectiveness depends on driver acceptance and operating environment. This paper investigates the environment-dependent behaviour of a preference-weighted eco-driving optimal control framework for electric vehicles in car-following scenarios. The energy penalty factor is varied to characterise the trade-off between energy efficiency and car-following performance across *urban*, *rural*, and *motorway* driving conditions. Performance is evaluated using total energy loss and RMS following error. Results show measurable energy reductions in all environments, but the trade-off structure differs markedly: urban driving provides a wide trade-off region, rural driving exhibits a distinct knee, and motorway driving presents a constrained region with limited achievable benefit. These findings demonstrate that while preference-weighted eco-driving is broadly effective, its trade-off characteristics are strongly environment dependent, and fixed weighting strategies may not yield uniformly optimal behaviour across mixed driving conditions.**

***Index Terms*—Eco-driving, electric vehicle, driver preference, energy loss, energy-efficient control..**

I. INTRODUCTION

The transportation sector is a major contributor to global energy consumption and greenhouse gas emissions, with passenger vehicles accounting for nearly half of the sector's impact [1]. Electrification of road transport has therefore emerged as a key pathway toward reducing tailpipe emissions [2]; however, the overall energy efficiency of electric vehicles (EVs) remains a critical concern due to limited driving range, charging constraints, and battery degradation considerations [3]. Beyond hardware-level improvements in batteries and electric drivetrains, driving behaviour has been shown to exert a substantial influence on vehicle energy consumption, making eco-driving an attractive and immediately deployable strategy for improving EV efficiency [4], [5].

Eco-driving aims to reduce energy losses by promoting smoother acceleration, anticipatory braking, and moderated speed profiles [6], [7]. In recent years, eco-driving has increasingly been formulated as an optimal control problem, enabling systematic generation of energy-efficient velocity trajectories while satisfying vehicle dynamics and operational constraints. "'latex Energy-efficient driving has been extensively treated as a longitudinal optimal control problem, in which vehicle dynamics, resistive road-load forces, and drivetrain-related energy losses are explicitly incorporated into the trajectory optimisation framework [8], [9]. In the context of electric vehicles, optimisation-based eco-driving has demonstrated notable reductions in energy consumption due to the combined effects of velocity smoothing and enhanced utilisation of regenerative braking [10]–[12].

However, purely energy-oriented eco-driving strategies often generate trajectories that deviate significantly from natural driving behaviour, resulting in overly conservative speeds or undesired acceleration patterns. Such behaviour can negatively impact driver acceptance and limit the practical applicability of eco-driving systems [5], [13]. To address this challenge, recent research has incorporated driver preference into eco-driving optimisation frameworks by explicitly modelling driver-preferred acceleration behaviour, desired cruising speed, and car-following behaviour within the control objective. Optimal-control-based formulations that integrate driver preference through car-following models have been shown to produce energy-efficient trajectories that remain consistent with naturalistic human driving behaviour [14]. By introducing a tunable weighting between energy efficiency and driver satisfaction, these approaches enable a flexible trade-off between energy-optimal operation and driver-oriented performance [15]. While driver-preference-based eco-driving frameworks have proven effective in reducing aggregate energy consumption, existing studies typically evaluate performance using a single standardised driving cycle or a limited set of scenarios. Consequently, fixed driver-preference weightings are often assessed through averaged energy savings, providing limited insight into how the same weighting behaves across different real-world driving contexts [11], [12].

In practice, EVs operate across diverse environments, including stop–start urban traffic, smoother rural roads, and motorway routes with sustained high-speed cruising. Previous studies have shown that dominant energy-loss mechanisms vary substantially with driving conditions: braking losses dominate in urban driving, whereas aerodynamic losses become increasingly significant at higher speeds [16]. Consequently, the interaction between driver-preference weighting and vehicle energy losses cannot be assumed to be uniform across environments. Motivated by these considerations, this paper investigates the environment-dependent behaviour of preference-weighted eco-driving in EV car-following scenarios. A multi-objective optimal control formulation from [15] is used to trade off driver-preferred car-following behaviour and total energy loss across different real-world driving environments. The focus in this work is on systematic analysis of how an identical control framework and energy penalty weighting interact with different real-world driving environments. Real-world driving

[1]All authors are with the Wolfson School of Mechanical, Electrical and Manufacturing Engineering, Loughborough University, LE113TU, Loughborough, UK s.qamar@lboro.ac.uk, p.hubbard@lboro.ac.uk, j.fleming@lboro.ac.uk

[2]Will Midgley is with the School of Mechanical and Manufacturing Engineering, UNSW Sydney, Australia w.midgley@unsw.edu.au

data are used to evaluate the resulting trajectories, and energy performance is assessed to quantify the impact of driver-preference weighting across different driving environments.

The main contributions of this paper are as follows:

- Investigation of the trade-off between minimising energy losses and maintaining naturalistic car-following behaviour in urban, rural, and motorway driving when using eco-driving optimisation with driver preferences.
- Demonstration that tuning the weighting parameter separately for urban, rural, and motorway scenarios can yield Pareto improvements for longer journeys involving a combination of these driving environments.

The remainder of this paper is organised as follows: Section II summarises the eco-driving optimal control formulation with driver preference integration for optimising the velocity profiles. Section III describes the driving environments and optimisation setup used in this study. Section IV discusses the simulation results across different driving environments, and Section V concludes the paper with key findings and directions for future work.

II. Eco-Driving Optimal Control Problem Formulation

Eco-driving is formulated as a multi-objective optimal control problem (OCP) incorporating both energy efficiency and driver-preference objectives in car-following scenarios. The objective is to achieve a balanced trade-off between maintaining the desired driving performance and minimising overall energy consumption. A composite cost function combines an energy-loss term L_{energy}, and a driver preference term L_{DSM}, in terms of speed and acceleration preferences.

A. Vehicle Dynamics and Energy Loss Model

The ego electric vehicle is modelled using a simplified longitudinal dynamics representation, considering the primary sources of energy loss. The vehicle is represented as a point mass subject to propulsion, braking, aerodynamic drag, and rolling resistance forces. The longitudinal motion is described by

$$\dot{v}(t) = u_m(t) + u_b(t) - \frac{1}{2m}\rho C_d A v^2(t) - gC_{rr}, \tag{1}$$

where $v(t)$ denotes the vehicle speed, $u_m(t)$ and $u_b(t)$ represent the motor and mechanical braking accelerations, respectively, m is the vehicle mass, ρ is air density, C_d is the aerodynamic drag coefficient, A is the frontal area, and C_{rr} is the rolling resistance coefficient. The inter-vehicle spacing $s(t)$ evolves according to

$$\dot{s}(t) = v(t) - v_L(t), \tag{2}$$

where $v_L(t)$ is the recorded lead-vehicle velocity.

The energy objective minimises the cumulative energy losses incurred during driving [8]. The instantaneous total energy loss is modelled as the sum of braking, aerodynamic, rolling resistance, and motor losses,

$$L_{\text{energy}} = L_{\text{brk}} + L_{\text{drag}} + L_{\text{rr}} + L_{\text{motor}}. \tag{3}$$

Substituting the expressions for each loss component gives

$$L_{\text{energy}} = -mu_b v + \frac{1}{2}\rho C_d A v^3 + mgC_{rr} v + R_m I_m^2. \tag{4}$$

The motor current, I_m is calculated as

$$I_{\text{m}} = \frac{m u_m r_w}{N_g k}, \tag{5}$$

where R_m, r_w, N_g, and k denote motor resistance, wheel radius, gear ratio, and motor torque constant, respectively. The energy-related cost over the optimisation horizon T is given by

$$J_E = \int_0^T L_{\text{energy}}(t)\, dt. \tag{6}$$

B. Driver Satisfaction Model

To maintain naturalistic car-following behaviour and support driver acceptance, a driver satisfaction model from [17] is incorporated into the cost function. In this work, driver preference primarily represents desired speed and following-distance tracking behaviour. The model also penalises excessive acceleration and braking effort, but the car-following terms are central to the interpretation of driver-preferred behaviour in this study. The driver satisfaction cost is expressed as

$$J_D = \int_0^T L_{\text{DSM}}(t)\, dt, \tag{7}$$

where L_{DSM} is a nonlinear function of acceleration effort, speed error, and spacing error.

$$L_{DSM} = \left(\frac{u_m}{a}\right)^2 + \left(\frac{u_b}{b}\right)^2 + \beta\left(\frac{v}{v_d} - 1\right)^2 + \frac{\gamma\left(\frac{s}{s_d} - 1\right)^2}{\left(\frac{s}{s_d}\right)^2 + 1}, \tag{8}$$

where u_m and u_b denote motor and braking accelerations, respectively. v_d is the desired free-flow speed, s_0 the minimum standstill gap, and T_0 the desired time headway. Parameters a and b characterise driver acceleration and braking behaviour, while s and v denote spacing and velocity. The desired spacing s_d is defined as

$$s_d = s_o + T_o v + \frac{v(v - v_L)}{2\sqrt{ab}} \tag{9}$$

β and γ are weighting parameters that trade off between the objectives, with details provided in [17]. When minimised in isolation, this formulation yields behaviour consistent with the Intelligent Driver Model (IDM) while remaining smooth and well-conditioned for optimal control.The above designed model of electric vehicle in OpenOCL has been validated to approximately match the Simulink model in [18].

C. Multi-Objective Optimal Control Problem

The complete eco-driving optimisation problem is formulated by combining the energy and driver satisfaction objectives through a weighting parameter $\alpha \in [0, 1]$ [15].

$$\min_{u_m, u_b} \; J = \int_0^T \left[\alpha L_{energy}(t) + (1 - \alpha) L_{DSM}(t)\right] dt \tag{10}$$

subject to system dynamics and the physical constraints

$$\dot{v}(t) = u_m(t) + u_b(t) - \frac{1}{2m}\rho C_d A v^2(t) - gC_{rr} \quad (11)$$

$$\dot{s}(t) = v(t) - v_L(t), \quad (12)$$

$$v(t) \geq 0, \quad s(t) \geq 0, \quad (13)$$

$$\underline{u}_m \leq u_m(t) \leq \overline{u}_m, \quad u_b(t) \leq 0. \quad (14)$$

By varying α, the framework enables a flexible trade-off between driver-preferred car-following behaviour ($\alpha = 0$) and energy-oriented eco-driving ($\alpha \to 1$). At low α, the optimiser prioritises reducing deviations from the desired following distance and lead-vehicle behaviour. At high α, it permits larger following-distance deviations in order to reduce energy losses.

III. Driving Environments and Evaluation Setup

The evaluation uses real-world driving data recorded from an on-road journey in Padova, Italy. The recorded velocity profile is segmented into representative operating regimes to analyse eco-driving behaviour under different traffic conditions, as follows:

- **Urban:** low speeds with frequent stop–start behaviour and repeated acceleration and deceleration.
- **Rural:** moderate speeds with smoother velocity variations and intermittent transients.
- **Motorway:** sustained higher speeds with comparatively limited speed modulation.

The recorded velocity profile is treated as the lead-vehicle trajectory, which the ego vehicle follows using the optimal control framework of Section II. For each environment, the OCP is solved over the corresponding horizon for multiple values of the energy penalty weighting parameter α. The resulting trajectories are evaluated using the same vehicle model and tracking controller within a car-following framework that enforces safe spacing via the driver satisfaction model. “‘latex

Performance is evaluated in terms of total energy loss and RMS following error, enabling the construction of environment-specific Pareto fronts. The RMS following error between actual and desired spacing is used to quantify the car-following performance. For a given driving segment k of duration T_k, the RMS following error is defined as

$$\mathrm{RMS}_k = \sqrt{\frac{1}{T_k}\int_0^{T_k} \left(s_k(t) - s_{d,k}(t)\right)^2 \, dt}, \quad (15)$$

To evaluate the complete drive cycle, the segment RMS errors are aggregated using a duration-weighted formulation, ensuring that longer segments contribute proportionally to the overall metric.

$$\mathrm{RMS}_{\text{tot}} = \sqrt{\frac{\sum_{k=1}^{N} T_k \, \mathrm{RMS}_k^2}{\sum_{k=1}^{N} T_k}} = \sqrt{\frac{1}{T_{\text{tot}}}\sum_{k=1}^{N} T_k \, \mathrm{RMS}_k^2}, \quad (16)$$

where $s_k(t)$ and $s_{d,k}(t)$ denote the actual and desired spacing in segment k, T_k is the segment duration, N is the number of segments, and $T_{\text{tot}} = \sum_{k=1}^{N} T_k$.

The formulated optimal control problem is solved offline using a direct collocation method implemented in OpenOCL [19], an open-source framework for optimal control. OpenOCL employs CasADi [20] for automatic differentiation and IPOPT [21] as the nonlinear solver.

IV. Results and Discussion

All simulations use a representative electric vehicle model based on the 2023 Toyota bZ4X Vision AWD configuration with identical parameters listed in Table I. This ensures that observed differences in energy consumption arise solely from the characteristics of the driving environment and the weighting of the preference of the driver.

TABLE I: Parameters of Ego Vehicle and Driver Model

Symbol	Parameter	Units	Value
m	Vehicle mass	kg	$2140 + 70$
A_f	Vehicle frontal area	m^2	2.6
ρ	Air density	kg/m^3	1.225
C_{rr}	Rolling resistance coefficient	–	0.01
C_d	Drag coefficient	–	0.291
r_w	Radius of wheel	m	0.365
g	Gravitational acceleration	m/s^2	9.81
N_g	Gear ratio	–	9.5
R_m	Armature resistance	Ω	1×10^{-3}
$P_{m,\max}$	Motor peak power	kW	80
$T_{m,\max}$	Motor maximum torque	Nm	168
k	Motor torque constant	Nm/A	0.8
a	Preferred acceleration	m/s^2	3
b	Preferred braking	m/s^2	4
s_o	Desired minimum gap between vehicles	m	2
v_d	Desired speed	m/s	30
T_o	Time headway	s	1

A. Urban Driving Environment

The optimisation results obtained for the urban driving scenario are presented in Fig. 1, for three representative values of the energy penalty parameter α, illustrating the shift from driver preference to energy efficiency. The complete trade-off between energy loss and car-following performance obtained from the full sweep of $\alpha = 0$–0.9 is shown by the Pareto front in Fig. 2. For $\alpha = 0$, the response is purely driver preference oriented, and the ego vehicle closely tracks the velocity of the lead vehicle, leading to pronounced acceleration activity and frequent braking. As the energy penalty factor increases, the optimisation progressively smooths the ego-vehicle velocity profile, reducing aggressive acceleration and braking behaviour while relaxing strict car-following requirements, as shown in Fig. 1.

Table II quantifies this trend: increasing the energy penalty factor produces substantial reductions in total energy loss, while the RMS following error increases, reflecting reduced adherence to driver-preferred following behaviour. The Pareto front in Fig. 2 shows that intermediate values of α achieve significant energy reductions with comparatively smaller increases in following error.

B. Rural Driving Environment

Fig. 3 shows the optimised velocity profiles for the rural drive cycle. Increasing the energy penalty factor α produces progressively smoother ego-vehicle trajectories, reflecting greater emphasis on energy efficiency.

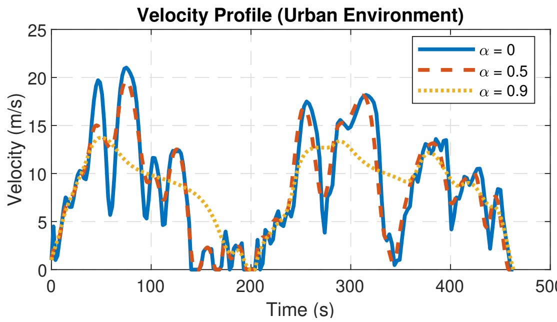

Fig. 1: Optimised velocity profiles of real-world urban drive cycle with varying energy penalty factor α

TABLE II: Urban drive cycle trade-off between total energy loss and car-following performance.

α	Total Energy Loss (kJ)	RMS Following Error (m)
0.0	962.42 (–)	0.91
0.1	910.59 (↓ 5.39%)	1.11
0.2	886.73 (↓ 7.86%)	1.58
0.3	849.23 (↓ 11.76%)	2.70
0.4	793.64 (↓ 17.53%)	5.15
0.5	740.08 (↓ 23.09%)	7.74
0.6	688.32 (↓ 28.48%)	10.46
0.7	641.34 (↓ 33.36%)	14.07
0.8	516.85 (↓ 46.29%)	29.52
0.9	395.70 (↓ 58.87%)	79.90

Table III shows that, in the rural scenario, reductions in total energy loss occur more gradually than in urban driving for small to moderate energy penalty values. However, beyond a certain range of the energy penalty factor $(0-0.5)$, further energy reductions are accompanied by a sharp increase in RMS following error. This behaviour is reflected in the Pareto front in Fig. 4 , which exhibits a distinct knee. Prior to this transition, moderate energy savings can be achieved with relatively small increases in following error. Beyond it, additional energy-oriented optimisation produces disproportionately large deviations from driver-preferred behaviour, as evident in Fig. 3 for the $\alpha = 0.9$ case.

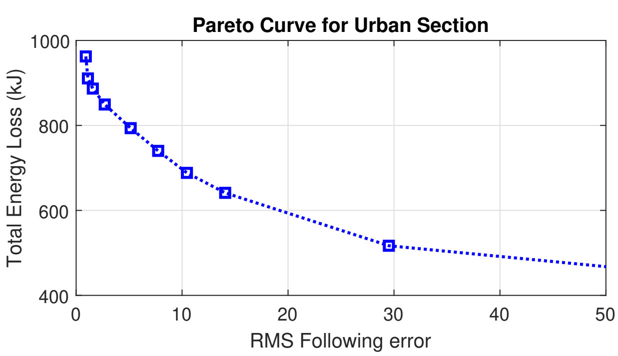

Fig. 2: Pareto fronts for the real-world urban drive cycle.

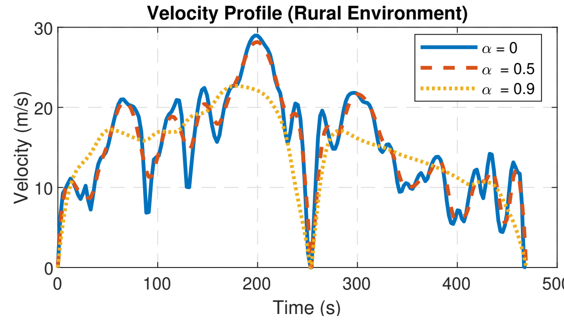

Fig. 3: Optimised velocity profiles of real-world rural drive cycle with varying energy penalty factor α

TABLE III: Rural drive cycle trade-off between total energy loss and car-following performance.

α	Total Energy Loss (kJ)	RMS Following Error (m)
0.0	2219.37 (–)	1.69
0.1	2108.28 (↓ 5.01%)	2.06
0.2	2032.71 (↓ 8.41%)	2.79
0.3	1952.53 (↓ 12.02%)	3.63
0.4	1906.03 (↓ 14.12%)	4.79
0.5	1840.48 (↓ 17.07%)	6.69
0.6	1574.38 (↓ 29.06%)	44.88
0.7	1530.53 (↓ 31.04%)	48.92
0.8	1503.22 (↓ 32.28%)	52.01
0.9	1352.84 (↓ 39.05%)	88.29

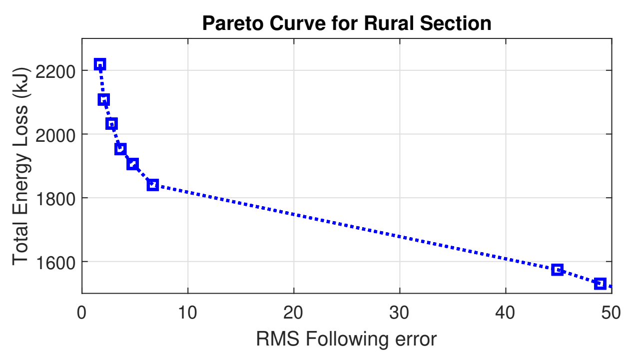

Fig. 4: Pareto fronts for the real-world rural drive cycle.

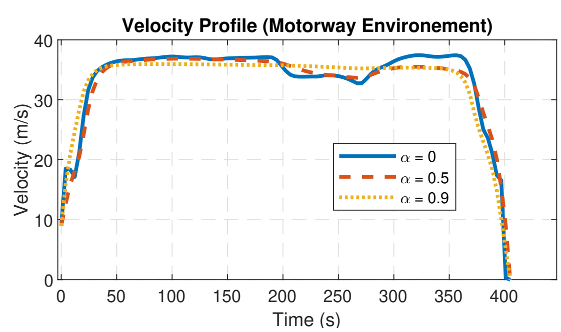

Fig. 5: Optimised velocity profiles of real-world motorway drive cycle with varying energy penalty factor α

TABLE IV: Motorway drive cycle trade-off between total energy loss and car-following performance.

α	Total Energy Loss (kJ)	RMS Following Error (m)
0.0	10480.57 (–)	12.80
0.1	10336.11 (↓ 1.38%)	12.97
0.2	10293.09 (↓ 1.79%)	13.60
0.3	9916.76 (↓ 5.38%)	53.64
0.4	9898.18 (↓ 5.56%)	54.59
0.5	9884.19 (↓ 5.69%)	55.19
0.6	9867.73 (↓ 5.85%)	56.29
0.7	9848.27 (↓ 6.03%)	58.63
0.8	9832.84 (↓ 6.18%)	75.26
0.9	9859.07 (↓ 5.93%)	92.83

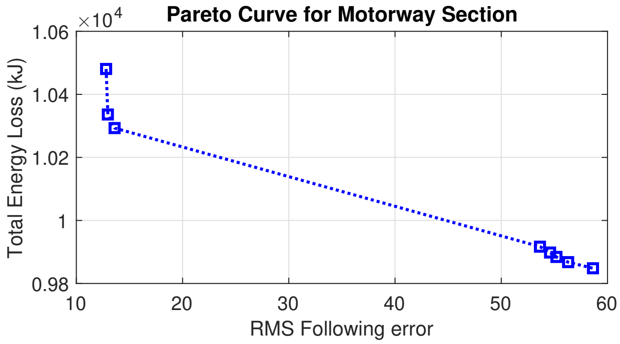

Fig. 6: Pareto fronts for the real-world motorway drive cycle.

C. Motorway Driving Environment

Fig. 5 shows the optimised velocity profiles for the motorway drive cycle. In contrast to the urban and rural scenarios, increasing the energy penalty factor α produces only minor changes in the ego-vehicle trajectory due to the predominantly steady cruising conditions.

Table IV shows that reductions in total energy loss remain relatively small across the range of α. However, RMS following error increases noticeably as the optimisation places greater emphasis on energy efficiency. This behaviour is reflected in the Pareto front in Fig. 6, which exhibits an early transition, indicating limited scope for favourable trade-offs between energy loss and car-following performance under sustained cruising conditions.

D. Mixed Driving Profile Analysis

A 25 km mixed driving profile including urban, rural and motorway segments was analysed to assess uniform versus segment-wise α selection. Fig. 7 presents the resulting Pareto distribution. The red curve corresponds to uniform-α values applied across all segments, while the coloured markers represent selected non-uniform configurations. α_u, α_r and α_m represent energy penalty factor for urban, rural and motorway segment respectively.

The green marker, corresponding to $(\alpha_u, \alpha_r, \alpha_m) = (0.3, 0.2, 0.1)$, reduces total energy loss from 11764.8 kJ (uniform $\alpha = 0.1$) to 11388.5 kJ, representing a 3.20% reduction, with only a marginal change in RMS following error (from 13.6 m to 13.8 m). Similarly, $(\alpha_u, \alpha_r, \alpha_m) = (0.3, 0.3, 0.1)$ achieves a 2.42% reduction in energy loss relative to uniform $\alpha = 0.2$, while the RMS following error changes minimally from 14.2 m to 14.3 m.

Another configuration, $(\alpha_u, \alpha_r, \alpha_m) = (0.4, 0.4, 0.2)$, also produces lower energy loss than the uniform-α Pareto front. These results indicate that a single fixed preference-weighting parameter may be suboptimal for mixed driving conditions. Allowing environment-dependent α selection enables more favourable global compromises between energy efficiency and car-following performance.

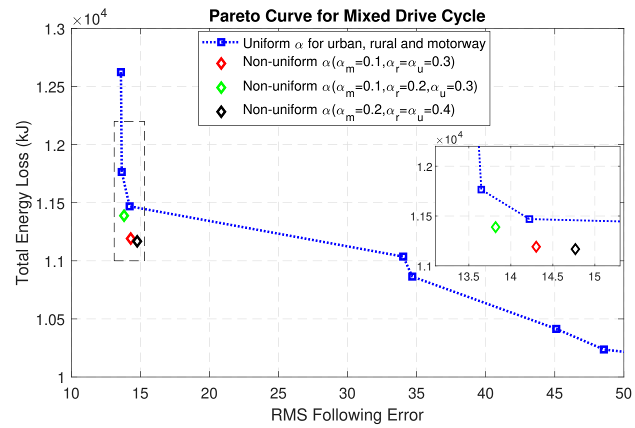

Fig. 7: Comparison of uniform and non-uniform preference weighting for the mixed drive cycle.

E. Discussion

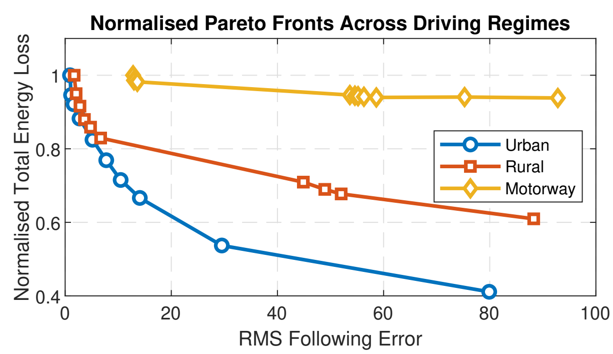

Fig. 8: Comparison of normalised Pareto fronts realtive to Naturalistic driving case($\alpha = 0$.

The normalised Pareto fronts relative to naturalistic driving ($\alpha = 0$) in Fig. 8 show differences in the trade-off between energy loss and car-following performance across driving environments. Urban driving exhibits the widest trade-off region due to frequent stop–start behaviour, rural driving shows a distinct knee indicating a limited favourable compromise, and motorway driving presents a narrow trade-off with comparatively small achievable energy reductions. The distributions in Fig. 9 quantify these trends, with urban driving achieving the largest energy reductions and motorway driving the smallest. These results indicate that preference-weighted eco-driving performance is affected by environment, suggesting that a

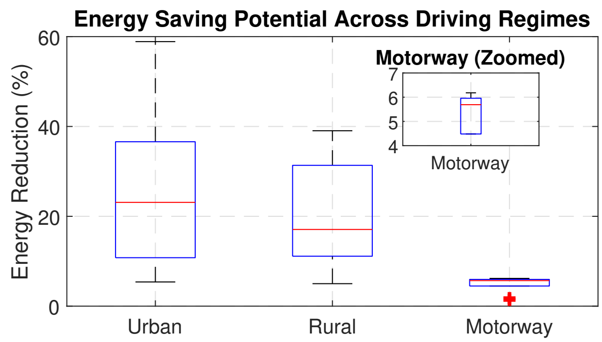

Fig. 9: Energy reduction across driving environments under varying energy–car-following trade-offs.

single fixed weighting parameter may therefore be suboptimal for mixed driving conditions. This is also evident from the mixed-drive-cycle analysis, where several environment-specific α selections produce solutions below the uniform-α Pareto curve.

This may occur because the optimisation minimises the driver satisfaction cost L_{DSM}, whereas the Pareto analysis uses RMS following error as a proxy for driver-preferred behaviour. Since these metrics differ, the plotted curves represent an empirical trade-off between energy loss and RMS following-distance error. Additionally, weighted-sum formulations recover only convex Pareto regions, so a single fixed weighting may not capture all favourable trade-offs. From a physical perspective, dominant loss mechanisms vary across environments: braking and motor losses dominate urban driving, while aerodynamic drag dominates motorway cruising. These observations support environment-dependent α selection for mixed real-world driving scenarios.

V. Conclusion

This paper investigated a preference-weighted eco-driving optimal control framework for electric vehicles operating in car-following scenarios. The proposed optimisation approach achieved measurable reductions in energy loss while maintaining controllable car-following behaviour, confirming the effectiveness of the eco-driving strategy. The framework was evaluated across urban, rural, and motorway driving environments using real-world driving data.

Energy savings were achieved in all cases, however, the resulting trade-offs between energy efficiency and driver-preferred car-following behaviour differed across environments, indicating that the achievable balance is strongly context dependent. Analysis of a mixed driving profile further showed that applying a single uniform weighting parameter across all segments does not necessarily yield the most favourable overall compromise. Allowing the preference-weighting parameter to vary between environments produced improved global solutions compared with uniform weighting.

These findings highlight the importance of adaptive weighting strategies when incorporating driver preference into eco-driving optimisation. Future work will focus on developing environment-aware eco-driving strategies capable of adjusting the preference-weighting parameter in real time.

References

[1] S. Wee, M. Coffman, and S. Allen, "EV driver characteristics: Evidence from Hawaii," *Transport Policy*, vol. 87, pp. 33–40, 2020.

[2] L. Hutchinson, B. Waterson, B. Anvari, and D. Naberezhnykh, "Potential of wireless power transfer for dynamic charging of electric vehicles," *IET Intelligent Transport Systems*, vol. 13, no. 1, pp. 3–12, 2018.

[3] S. Kim, J. Lee, and C. Lee, "Does driving range of electric vehicles influence electric vehicle adoption," *Sustainability*, vol. 9, no. 10, p. 1783, 2017.

[4] A. E. af Wåhlberg, "Long-term effects of training in economical driving," *International Journal of Industrial Ergonomics*, vol. 37, no. 4, pp. 333–343, 2007.

[5] B. Beusen, S. Broekx, T. Denys, C. Beckx, B. Degraeuwe, M. Gijsbers, K. Scheepers, L. Govaerts, R. Torfs, and L. I. Panis, "Using on-board logging devices to study the longer-term impact of an eco-driving course," *Transportation Research Part D: Transport and Environment*, vol. 14, no. 7, pp. 514–520, 2009.

[6] X. Zhao, Y. Wu, J. Rong, and Y. Zhang, "Development of a driving simulator based eco-driving support system," *Transportation Research Part C: Emerging Technologies*, vol. 58, pp. 631–641, 2015.

[7] J. N. Barkenbus, "Eco-driving: An overlooked climate change initiative," *Energy policy*, vol. 38, no. 2, pp. 762–769, 2010.

[8] A. Sciarretta, G. D. Nunzio, and L. L. Ojeda, "Optimal ecodriving control: Energy-efficient driving of road vehicles as an optimal control problem," *IEEE Control Systems Magazine*, vol. 35, no. 5, pp. 71–90, 2015.

[9] A. Sciarretta and A. Vahidi, *Energy-Efficient Driving of Road Vehicles*. Springer, 2020.

[10] M. Kuriyama, S. Yamamoto, and M. Miyatake, "Theoretical study on eco-driving technique for an electric vehicle with dynamic programming," in *Proceedings of the International Conference on Electrical Machines and Systems*, 2010, pp. 2026–2030.

[11] D. Shen, D. Karbowski, and A. Rousseau, "A minimum principle-based algorithm for energy-efficient eco-driving of electric vehicles," *IEEE Transactions on Intelligent Vehicles*, vol. 5, no. 4, pp. 725–737, 2020.

[12] P. Liao, T.-Q. Tang, R. Liu, and H.-J. Huang, "An eco-driving strategy for electric vehicles based on the powertrain," *Applied Energy*, vol. 302, p. 117583, 2021.

[13] X. Yan, C. Allison, J. Fleming, N. Stanton, and R. Lot, "The benefit of assisted and unassisted eco-driving for electrified powertrains," *IEEE Transactions on Human-Machine Systems*, vol. 51, no. 4, pp. 403–407, 2021.

[14] J. Fleming, X. Yan, C. Allison, N. Stanton, and R. Lot, "Driver modeling and implementation of a fuel-saving ADAS," in *IEEE International Conference on Systems, Man, and Cybernetics*, 2018, pp. 1233–1238.

[15] S. Qamar, P. Hubbard, W. Midgley, and J. Fleming, "Optimal eco-driving and user preference integration for enhanced energy efficiency in awd electric vehicles," in *2025 International Conference on Control, Automation and Diagnosis (ICCAD)*, 2025, pp. 1–6.

[16] Y. Al-Wreikat, C. Serrano, and J. R. Sodré, "Driving behaviour and trip condition effects on the energy consumption of an electric vehicle under real-world driving," *Applied Energy*, vol. 297, p. 117096, 2021.

[17] J. Fleming, X. Yan, and R. Lot, "Incorporating driver preferences into eco-driving assistance systems using optimal control," *IEEE trans. on Intelligent Transportation Systems*, vol. 22, no. 5, pp. 2913–2922, 2020.

[18] S. Qamar, P. Hubbard, W. Midgley, and J. Fleming, "Validation of an OpenOCL model for energy efficient electric vehicle control," in *2024 UKACC 14th International Conference on Control (CONTROL)*, 2024, pp. 219–220.

[19] J. Koenemann, G. Licitra, M. Alp, and M. Diehl, "Openocl – open optimal control library," 2017, https://github.com/OpenOCL/OpenOCL.

[20] J. A. Andersson, J. Gillis, G. Horn, J. B. Rawlings, and M. Diehl, "Casadi: A software framework for nonlinear optimization and optimal control," *Mathematical Programming Computation*, vol. 11, no. 1, pp. 1–36, 2019.

[21] A. Wächter and L. T. Biegler, "On the implementation of an interior-point filter line-search algorithm for large-scale nonlinear programming," *Mathematical Programming*, vol. 106, no. 1, pp. 25–57, 2006.